TOWARDS MASSIVELY PARALLEL LARGE EDDY SIMULATION OF TURBINE STAGES

Gaofeng WANG*, Dimitrios Papadogiannis, Florent Duchaine, Nicolas Gourdain, Laurent Y.M. Gicquel
Computational Fluid Dynamics Team, CERFACS 42, avenue G. Coriolis, 31057 Toulouse Cedex 1, France
Email address: laurent.gicquel@cerfacs.fr

ABSTRACT

The context of integrated numerical simulations of gas turbine engines by use of high-fidelity Computational Fluid Dynamic (CFD) tools recently emerged as a promising path to improve engines design and understanding. Relying on massively parallel super-computing such propositions still have to prove feasibility to efficiently take advantage of the ever increasing computing power made available worldwide. Although Large Eddy Simulation (LES) has recently proven its superiority in the context of the combustion chamber of gas turbine, methodologies need to be developed and start addressing the problem of the turbomachinery stages, if integrated simulations based on LES are to be foreseen. In the proposed work an in-house code and strategy, called TurboAVBP, is developed for turbomachinery LES thanks to the coupling of multi-copies of the unstructured compressible reacting LES solver AVBP, designed to run efficiently on high performance massively parallel architectures. Aside from the specificity of such wall bounded flows, rotor/stator LES type simulations require specific attention and the interface should not interfere with the numeric scheme to preserve proper representation of the unsteady physics crossing this interface. A tentative LES compliant solution based on moving overset grids method is proposed and evaluated in this work for high-fidelity simulation of the rotor/stator interactions. Simple test cases of increasing difficulty with reference numerical are detailed and prove the solution in handling acoustics, vortices and turbulence. The approach is then applied to the QinetiQ MT1 high-pressure transonic turbine for comparison with experimental data. Two configurations are computed: the first one is composed of 1 *scaled stator section and* 2 *rotors while the second computation considers the geometrically accurate periodic quarter of the machine, i.e.* 8 *stators and* 15 *rotors to test scalability issues of such applications. Although under-resolved, the LES pressure profiles on the stator and rotor blades appear to be in good agreement with experimental data and are quite competitive compared to the traditional (Unsteady) Reynolds-Averaged Navier-Stokes (RANS or URANS) modeling approach. Unsteady features inherently present in these LES underline the complexity of the flow in a turbine stage and clearly demand additional diagnostics to be properly validated.*

Nomenclature

Δt	physical time step
$\Delta x+$	cells size at wall along stream-wise direction
$\Delta y+$	cells size at wall along normal direction
$\Delta z+$	cells size at wall along span-wise direction
δ	wave characteristic length
$\Delta_x, \Delta_x^A, \Delta_x^B$	mesh size
Γ	vortex strength
$\mathbb{R}_{\Omega_j}$	residuals of cell Ω_j
$\mathbf{U}$	velocity vector
$\mathbf{W}$	conservative variables $(\rho, \rho\mathbf{U}, \rho E)$
$\mathfrak{L}$	interpolation operator
ν_t	turbulent viscosity
ϕ_i	shape functions
Ψ	stream function
ρ	density
ρ_0	ambient density
$\vec{\mathcal{F}}$	flux tensor $(\mathbf{F}, \mathbf{G}, \mathbf{H})^T$
c_0	ambient sound speed
D	diameter of cylinder or tube
E	energy
f	Lagrange polynomial function
$g(x)$	Gaussian function
P	pressure
P'	pressure perturbation
P^A	amplitude of pressure perturbation
P_0	ambient pressure
q_i	vertices i of cell

*Address all correspondence to this author. Email address: wang@cerfacs.fr

R_c	vortex characteristic radius
Re	Reynolds number
t	time
u'	velocity perturbation
u^A	amplitude of velocity perturbation
U_0	velocity of inflow
V_{Ω_j}	volume of cell Ω_j
x, y	Cartesian coordinates
$y+$	dimensionless wall distance
Ω_j	cell j
$\partial\Omega_j$	boundary of cell j
$D^k_{\Omega_j}$	distribution matrix
V_k	volume of node k

INTRODUCTION

Computational Fluid Dynamics (CFD) is and will remain a critical tool for the design of current and next generation gas turbine engines, targeting high efficiency, high power to weight ratio and high reliability. Two crucial components of a gas turbine, *i.e.* the compressor and the turbine, rely on parts where the flow goes around blades that are successively rotating (rotors) and fixed (stators), and depend on the objective they can either apply or extract work from the flowing gas. Current industrial turbomachinery simulations usually use Reynolds-Averaged Navier-Stoke (RANS) or Unsteady RANS (URANS) which rely on turbulence statistically stationary models to predict the mean flow fields of these individual elements. For rotor/stator interactions, URANS is necessary to hope capturing the unsteady deterministic interactions that are present in these configurations [1]. Today the computational cost of RANS or URANS is quite acceptable for engineering applications and explains their daily use in real applications. However such tools show limits whenever used to test off-design points computations [2], which is one limit that engineers need to face to keep improving the devices. The main reason for such limitations stems from the observation that rotating flows present in real machines are inherently unsteady and fully turbulent with transitions and separations that are often triggered by interactions between large and small flow scales.

With the rapid development of High Performance Computing (HPC), recent efforts have been made on the prediction of these complex turbulent flows around isolated parts by use of the high-fidelity Large Eddy Simulation (LES) modeling approach (review by Tucker [3]). Although much more computationally intensive, the hope is that LES can alleviate the modeling efforts by explicitly resolving the large flow structure temporal and spatial evolutions and by filtering out the smaller easier to model turbulent sub-grid structures. Preliminary demonstrations show that LES can resolve flows with transitions, separations thereby improving heat transfer predictions on structured or unstructured meshes [4–6]. Tip-clearance flow predictions [7] have also be addressed successfully with LES. Nowadays, high performance massively parallel CFD solvers have reported capacity of handling up to 21 billion unstructured tetra cells with a very reasonable speedup: $16,000$ times faster than a single-processor performance if used in parallel on $32,786$ processors [8]. Following the analysis of Tucker [9], this capability seems to be approaching the requirements of most gas turbine applications. McMullan *et. al.* [2] have also demonstrated that LES can accurately predict the surface pressure on the Monterey cascade with a sufficiently refined mesh. Applicability in real machines is currently investigated and two configurations of compressor stages have been reported [2]: a scaled last stage of the Cranfield BBR compressor with a Reynolds number of $Re = 180,000$ and the Cambridge axial compressor ($Re = 350,000$). In parallel, LES has demonstrated its capacities in predicting the turbulent reacting flow in the combustor [10,11] where it is emerging today as a design tool in industry. Ultimately and within few decades, it may be of interest to address fully coupled compressor/combustor or combustor/turbine with LES, considering the ever increasing computing power and the use of massively parallel computers.

Today only few research groups have reported LES of compressor or turbine stages for three reasons:

1 the high computational costs related to such complex flows with high Reynolds numbers $Re \sim O(10^{6-7})$,
2 the still present difficulty of adequately resolving the wall flow, which is known to have a dramatic impact on the main vein flows (and vice-versa) and finally,
3 the capacity of current LES codes to adequately handle rotating interfaces with the required accuracy, *i.e.* resolved vortices, acoustic waves and turbulence should travel across the interface without being altered by the numerical treatment to preserve the LES nature of the solver in this region.

The last point is crucial and in fact rarely discussed or validated. In an attempt to provide validation of the interface treatment for LES of turbomachinery, this work proposes to study a coupling interface based on overset grids for LES of turbomachinery stages. The overset grid method has originally been proposed for Computational AeroAcoustics (CAA) [12], coupling CFD/CAA [13] codes to handle complex geometries [4] with very high accuracy [14,15]. It has also been used in RANS of external and turbomachinery flows where it is commonly known as the Chimera method [16] and reported as providing an equivalent accuracy as the sliding mesh method [17]. In the specific RANS context, conservativity is sufficient since it guaranties boundness and numerical convergence towards the steady state solution of the problem. The numerical requirement is hence limited to the interpolation scheme on the interface surface meshes that needs to be conservative (normally taking first-order area-based interpolation) [18]. For LES, most of flow structures are resolved and should be transferred through the interface with as less influence as possible to preserve flow coherence, evolution as well as the numerical properties of the scheme. It is indeed crucial to

transport the information at the right physical speed across the interface without dissipating the structures. In this specific context, the overset grid method may be interesting as increasing its accuracy is straightforward [4, 12–15]. In the following the rotating interface is implemented based on this reported method in an unstructured compressible high-performance parallel LES solver (AVBP) and validated on increasingly complex test cases. This approach is then applied to simulate a high pressure turbine (QinetiQ MT1 turbine [19]), which is characterized by both high Reynolds and Mach numbers.

The paper is organized as follows: first the coupling and associated numerics are detailed in Section 1; validation cases are outlined and discussed in Section 2; preliminary use of the developed methodology is then presented prior to the analyses and discussion about the applications in Section 3; finally, conclusions and remarks are provided in Section 4.

1 NUMERICAL METHOD AND IMPLEMENTATION

The objective of the present section is to provide a description of the numerical methods retained for the treatment of the rotor/stator interface using the overset grid method. First governing equations, numerical schemes and formalisms present in the CFD code are recalled followed by the presentation of the numerical treatment introduced to treat the exchange of information at the interface.

Governing equations

The filtered unsteady compressible Navier-Stokes equations for LES that describe the spatially filtered mass, momentum and energy $(\rho, \rho\mathbf{U}, \rho E)$ conservations, can be written in the following conservative form:

$$\frac{\partial \mathbf{W}}{\partial t} + \vec{\nabla} \cdot \vec{\mathscr{F}} = 0, \tag{1}$$

where $\mathbf{W}$ is the vector containing the conservative variables $(\rho, \rho\mathbf{U}, \rho E)^T$ and $\vec{\mathscr{F}} = (\mathbf{F}, \mathbf{G}, \mathbf{H})^T$ is the flux tensor. For convenience, the flux is divided into two components:

$$\vec{\mathscr{F}} = \vec{\mathscr{F}}^C(\mathbf{W}) + \vec{\mathscr{F}}^V(\mathbf{W}, \nabla\mathbf{W}) \tag{2}$$

where $\vec{\mathscr{F}}^C$ is the convective flux depending on $\mathbf{W}$ and $\vec{\mathscr{F}}^V$ is the viscous flux depending on both $\mathbf{W}$ and its gradients $\nabla\mathbf{W}$. The contributions of Sub-Grid Scale (SGS) turbulence models are included in the viscous flux through the addition of the so called turbulent viscosity ν_t.

Numerical schemes

The governing equations are solved by the unstructured compressible LES solver, AVBP [20]. Three numeric schemes are proposed in the solver: Lax-Wendroff (LW, with 2nd-order accuracy in time and space) which is a finite volume scheme [21] and the two-step Taylor-Galerkin finite element schemes TTG4A [22] and TTGC [23] (with 3rd-order in time and space). All schemes are expressed in the cell-vertex numerical discretization method, for its compactness and effectiveness on parallel HPC. With such numerics the cell-based residuals, *i.e.* the spatially dependent terms of the equations for each control volume Ω_j, are calculated by integrating the fluxes over the cell as:

$$\mathbb{R}_{\Omega_j} = \frac{1}{V_{\Omega_j}} \int_{\partial\Omega_j} \vec{\mathscr{F}} \cdot \vec{n} dS, \tag{3}$$

where V_{Ω_j} is the cell volume and $\partial\Omega_j$ its boundary with normal vector $\vec{n}$. Since the integration is obtained around a vertex, a distributed version of these cell-based residuals $\mathbb{R}_k$ is constructed via distribution matrices. One can hence express Eq. (1) into the semi-discrete scheme

$$\frac{d\mathbf{W}_k}{dt} = \mathbb{R}_k = -\frac{1}{V_k} \sum_{j|k\in\Omega_j} D^k_{\Omega_j} V_{\Omega_j} \mathbb{R}_{\Omega_j}, \tag{4}$$

where $D^k_{\Omega_j}$ is the distribution matrix that weights the cell residual from the cell center Ω_j to node k and V_k is a control volume associated to each node.

In static (no moving interface) parallel computations, the computational domain is divided into several individual vertices-shared partitioned domains each of which is attributed to one processor using Domain Decomposition Methods (DDM). Figure 1a illustrates the DDM coupling process for a cell-vertex scheme. In this illustration, the cells $(\mathbf{L_{1,2}}, \mathbf{R_{1,2}})$ are grouped into two domains respectively denoted by $\mathbf{L}$ and $\mathbf{R}$ having one common node $\mathbf{a}$. In such schemes, the cell-based residuals are computed locally (*i.e.* for all individual cells) and scattered to the belonging vertices. Vertex $\mathbf{a}$ which is located on the interface therefore needs all the contributions from the neighboring partitions for the nodal residual to be evaluated following Eq. (4). In conventional approaches of static massively parallel codes, this can be done simply through network communications.

Overset method for rotor and stator computations

The problem for the rotor/stator coupling may be similar to the DDM described above, except that the two domains $\mathbf{L}$ and $\mathbf{R}$ are moving (rotating) relative to each other. Non-conformal vertices (shown in Fig. 1b) are hence present at the interface and need therefore additional evaluations at every iteration when compared to static DDM. Numerically, several coupling methods are possible. ① Coupling fluxes before computing the cell-based

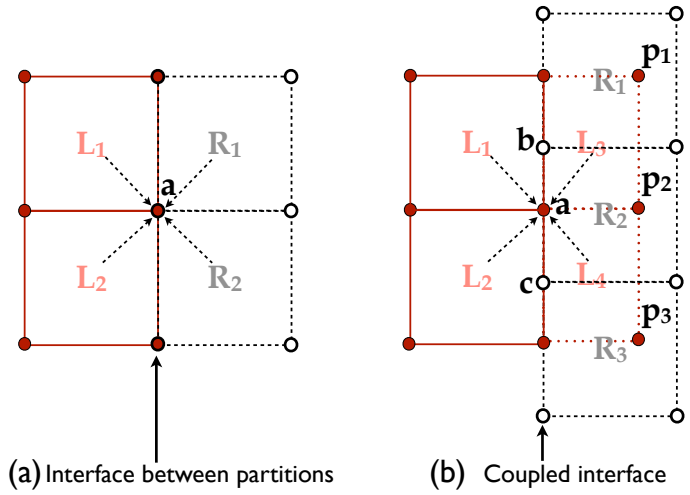

FIGURE 1. DDM for cell-vertex schemes used in parallel computations (a) and the proposed method for rotor/stator interface (b). $\mathbf{L_{1,2,3,4}}$ (composed of: hard lines – edges and filled symbols – vertices) and $\mathbf{R_{1,2,3}}$ (composed of: dashed lines – edges, vertices – empty symbols) denote the cells on the left and right sides of a partitioned domain, respectively. In the car of a moving fluid boundary, points $\mathbf{a}$ of domain $\mathbf{L}$ and points $\mathbf{b},\mathbf{c}$ of domain $\mathbf{R}$ are the vertices to be coupled since at the interface. Points $\mathbf{p_{1,2,3}}$ and $\mathbf{L_{3,4}}$ are additional vertices involved in the coupling when the overlap method is introduced.

residuals of Eq. (3) has the benefit of involving only the interface nodes. The computed fluxes should then be interpolated on the $2D$ coupled interface as performed in the traditional sliding mesh approach [18]. An alternative is ② coupling nodal residuals. In this approach, each nodal residual $\mathbb{R}_a^L$, $\mathbb{R}_b^R$ and $\mathbb{R}_c^R$ is calculated by counting the contributions of all sub-domain local cells using Eq. (4). Then the contributions of each domain missing in the other domain are estimated by introducing an additive interpolation $\mathfrak{L}$ to obtain the vertex $\mathbf{a}$ residual at the interface for example,

$$\mathbb{R}_a = \mathbb{R}_a^L + \mathfrak{L}(\mathbb{R}_b^R, \mathbb{R}_c^R). \tag{5}$$

With this approach the difficulty is the additive interpolation algorithm which evolves with time and is not easily accessible. This approach was in fact found to be unstable in the case of two rotating domains with the use of simple linear and nearest neighbor interpolation schemes. The remaining solution retained in the following consists in ③ reconstructing the residuals using an overset grid method, exchanging by interpolation the multi-domain conservative variables. As shown in Fig. 1b, overset grids rely on extending domain $\mathbf{L}$ by two $\mathbf{L_{3,4}}$ or more ghost cells so that the nodal residual of vertex $\mathbf{a}$ can be computed from cell-based residuals of $\mathbf{L_{1,2,3,4}}$ using the conservative variables needed to evaluate the right-hand side of Eq. (3). Cells $\mathbf{L_{3,4}}$ are

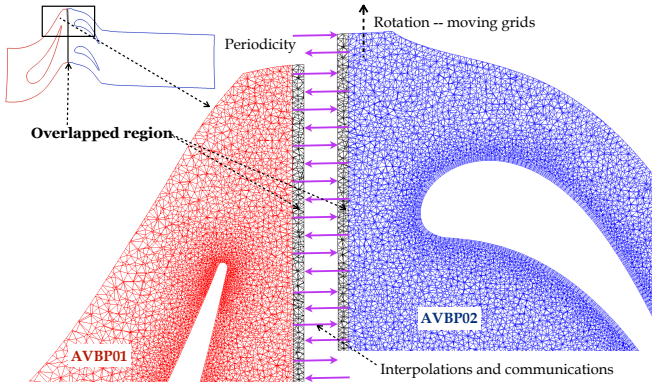

FIGURE 2. Communications framework of coupling rotor/stator interface.

geometrically overlapped with the domain $\mathbf{R}$ with points located in cells $\mathbf{R_{1,2,3}}$. Note that in the more generic cases the extent and topology of the duplicated cells will not coincide. The unknown conservative variables of the overset vertices $\mathbf{p_{1,2,3}}$ are then approximated through an interpolation of the information of cells $\mathbf{R_{1,2,3}}$. The same procedure is used to compute the nodal residuals of $\mathbf{b},\mathbf{c}$ at domain $\mathbf{R}$ which is also extended onto mesh $\mathbf{L}$ by two cells, since it is a two-way coupling. This third approach is chosen as it is easily implemented externally from the base CFD code and yields high-order accuracy if used in conjunction with higher order interpolation [12–15, 24].

In the implementation, a Lagrange interpolation operator can be used for exchanging the conservative variables of the overset nodes following:

$$\mathfrak{L}f = \sum_{i=1}^{n_{sh}} f(q_i)\phi_i \tag{6}$$

where f is a function approximated by Lagrange polynomial elements and $f(q_i)$ are the function values at the vertices q_i; n_{sh} is the number of freedoms of the element and ϕ_i are its shape functions. For nodes in an element, the interpolation coefficients are calculated based on the shape functions using the local coordinates of the elements. The implementation details of the interpolation routine includes: (1) find the enclosed cell; (2) calculate the local coordinates in the cell; (3) calculate the interpolation coefficients using a shape function; (4) calculate the interpolated value using Eq. (6). In the current study, simple linear shape function, *i.e.* barycenter interpolation or bilinear interpolation, is used in agreement with $\mathbb{P}_1$ (triangular in 2D and tetra in 3D) and $\mathbb{Q}_1$ (quad in 2D and hexa in 3D) elements, implying an order of 2. The implementation [25] is compatible with the CGNS interpolation tool [26]. Finally, note that a high order interpolation is viable for unstructured meshes by introducing high order shape

functions [12–15, 24, 27].

In terms of methodology and overall strategy to extend the available LES solver to deal with rotor/stator simulations, external code coupling is preferred. Hence two or more copies of the same LES solver (namely AVBP) each with their own computational domain and static DDM algorithm, are coupled through the parallel coupler OpenPALM [25]. Figure 2 typically shows the communication framework for a rotor/stator coupling approach using the overset grid method described above. For this case, the whole flow domain should initially be divided into static (AVBP01) and rotating parts (AVBP02). For rotating parts, the code uses the moving-mesh approach [28] in the absolute frame of reference while the remaining unit simulates the flow in the non-rotating part in the same coordinate system. The interfaces between the two units involving rotating and non-rotating parts are coupled, as explained before with the overset grids by exchanging and interpolating the conservative variables wherever needed. To do so an efficient distributed search algorithm is implemented in the coupler OpenPALM to locate the points in parallel partitioned mesh blocks. This coupling algorithm will then update at each time step the information and carry the interpolation from one MPI world to the next and vice-versa. Issues of numerical stability of the coupled solution and the well-posed problem are directly linked to the size of the overlapped region and the stencil of the schemes. Although not developed here, one layer of vertices is required across the interface for the LW scheme while TTGC and TTG4A require four layers of vertices on each sides of the interface.

2 VALIDATION TEST CASES

Prior to the application of the proposed solution for high fidelity LES of rotor/stator problems, three validation cases are conducted focusing on acoustics, convection of a vortex and turbulence. Each case is run twice: the first computation constitutes the benchmark solution using one standard AVBP remming on one mesh, while the second computation uses two non-conformal overlapping meshes to evaluate the proposed coupling strategy. The primary objective is to qualify and quantify potential errors introduced by the coupling.

Acoustic wave

The first validation case is the simple problem of a $1D$ propagating acoustic wave (Euler equations) in an infinite domain. Figure 3 illustrates the configuration for the reference and coupled simulations. In the latter, two overlapping $1D$ meshed lines are computationally communicating using the overset interface approach described above. In the overlapped region, the meshes are non-coincident and the vertices from one mesh are located at the center of the corresponding cell from the other mesh. The conservative variables are coupled over four layers of nodes on each side and will be updated based on the interpolated values of the other mesh for each time step.

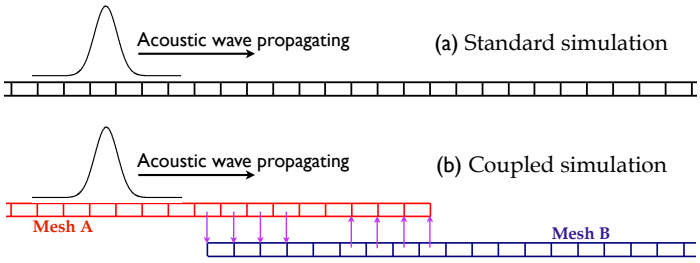

FIGURE 3. $1D$ acoustic wave propagation problem simulated by both approaches: (a) the standard standalone solver and (b) the equivalent coupled approach.

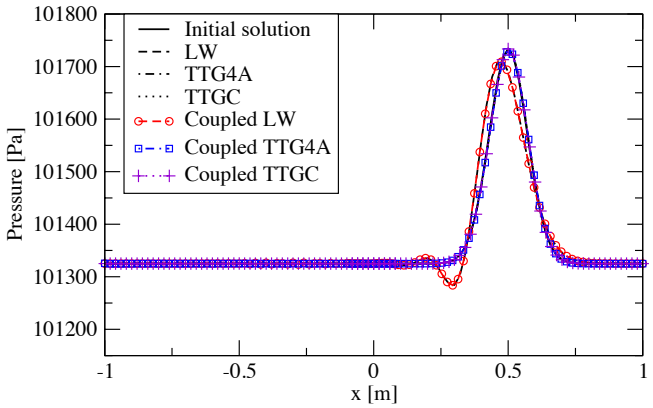

FIGURE 4. Pressure profiles in the computational domain obtained numerically after the wave has gone through the overlapped interface. The results from coupled simulations and standard simulations are provided for different numerical schemes.

To initialize this problem, an acoustic perturbation is centered at $x_0 = -0.5$ and has a Gaussian shape $g(x) = exp(-\frac{(x-x_0)^2}{\delta^2})$:

$$P' = \rho_0 c_0 u^A g(x) = P^A g(x) \tag{7}$$

where the amplitude of velocity perturbation $u^A = 1\ m/s$, corresponding to a pressure perturbation of $P^A = 388\ Pa$. Mean conditions are chosen to be at atmospheric conditions with zero mean flow. The characteristic length δ of the perturbation is chosen to equal $0.1\ m$, corresponding to a perturbation acoustic wave frequency of $3.4\ kHz$. All meshes are uniform with a spatial resolution of $\Delta_x = \delta/5 = 0.02\ m$. Three numerical schemes (LW, TTG4A and TTGC) are tested here. Figure 4 shows the pres-

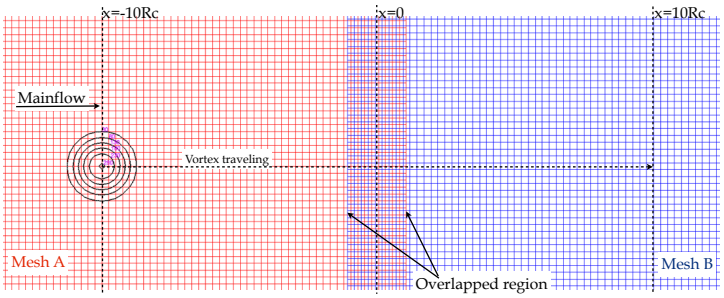

FIGURE 5. Schematic of coupled simulation of vortex traveling. Entire mesh A has 84x80 quad cells at rectangular domain of ($-20R_c$,-$10R_c$) to (R_c, $10R_c$) and mesh B has 84x81 quad cells at rectangular domain of ($-1.125R_c$,$-10R_c$) to ($20R_c$, $10R_c$). R_c is the radius of the initialized vortex.

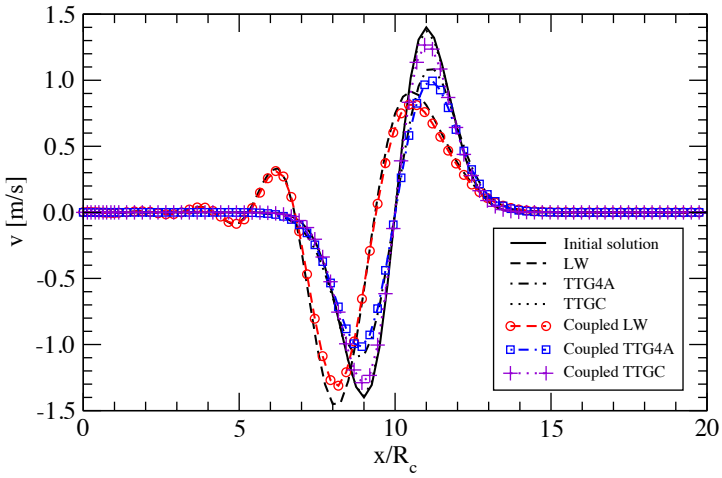

FIGURE 6. Transverse velocity v profiles over the distance in centerline along the main flow direction, at time $20R_c/U$.

sure profiles when the wave has reached the center of the second half domain ($x = 5\delta = 0.5\ m$). Compared to the analytical solution (initial profile translated at the speed of sound), the different schemes provide different standalone simulations' results representative of each scheme's properties (dissipation and phase-dispersion) that can then be compared to the coupled simulation. As illustrated by this test case, the standalone standard approach or coupled overset grid method clearly provide similar results, confirming that this recommended setup and strategy is consistent with the numerical schemes usually available for LES.

Inviscid traveling vortex

In general LES relies on its ability to resolve and transport vortices within a complex geometry. The second validation case is thus chosen to simulate a $2D$ vortex traveling through an overlapped interface using the Euler set of equations, so as to give access to potential interactions between the coupling procedure and a more complex flow. The numerical setup and the coupled computational domain are given in Fig. 5. It consists of two rectangular boxes with an overlapped region. For this computation, the first box is meshed by 84×80 quad cells and the second one has 84×81 quad cells. To prevent effects from the boundary conditions, all lateral surfaces are set to be periodic. To ensure convection of the initial vortex a mean flow, going from left to right, is also imposed. Concerning the details of the coupled approach, settings are similar to the previous test case, *i.e.* coupling through the overlapped interface with four layers of cells on each side of the interface. Likewise, the overlapped vertices are located at the center of the quad cells of the other mesh.

For this problem an initial isentropic vortex based on the stream function [29] expression is used,

$$\Psi(x,y) = \Gamma e^{-r^2/2R_c^2}, \tag{8}$$

where Γ is the vortex strength,r is the geometric distance to the vortex core ($x = -10\ R_c$) with R_c controlling the size of the vortex. The parameter set are $\Gamma = 0.0036\ m^2/s$, $R_c = 0.0156\ m$ (resulting in maxium variations of $u_{max} = v_{max} = 1.4\ m/s$ on velocity components). This field is being imposed on the top of a constant inflow $U_0 = 10\ m/s$ at atmospheric pressure $P_0 = 101,300\ Pa$. The mesh characteristic sizes are: $\Delta_x^A = R_c/4$ for the left mesh and $\Delta_x^B = R_c/4.05$ for the right one, as shown in Fig. 5.

For assessment, the transverse velocity component, v, is measured along a line of $y = \frac{1}{2}\Delta_x^B$ close to the centerline of the computational domain, when the vortex has reached the center of right mesh ($x = 10R_c$). Figure 6 compares the profiles between standard simulations , *i.e.* a single domain with 160×80 quad cells and a rectangular domain $(-20R_c, -10R_c) \times (20R_c, 10R_c)$, and the corresponding coupled simulations. Compared to the $1d$ test case, the coupled simulations have some additional dissipation (although very low) if compared to standard standalone domain predictions.

Turbulent pipe flow

This last validation test case focuses on a more relevant LES type of flow configuration: *i.e.* a fully turbulent flow containing a large range of energetic length scales evolving in time and space. The retained flow, often used to validate LES models and schemes, is a $3D$ turbulent pipe flow of diameter $D = 3$ mm, a bulk velocity of $U_0 = 100\ m/s$, resulting in a Reynolds number of $Re = 20,000$. Figure 7 illustrates the configuration for the coupled simulation, where two tubular domains are meshed using tetrahedric elements and coupled together with an overlap region. The length of each tube is $8\ D/3$ and the overlapped region

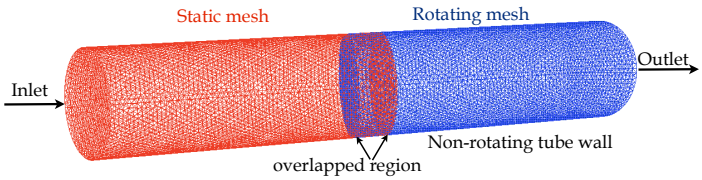

FIGURE 7. Coupled simulation of a turbulent pipe flow, $Re = 20,000$. The second mesh is rotating and coupled with the first mesh.

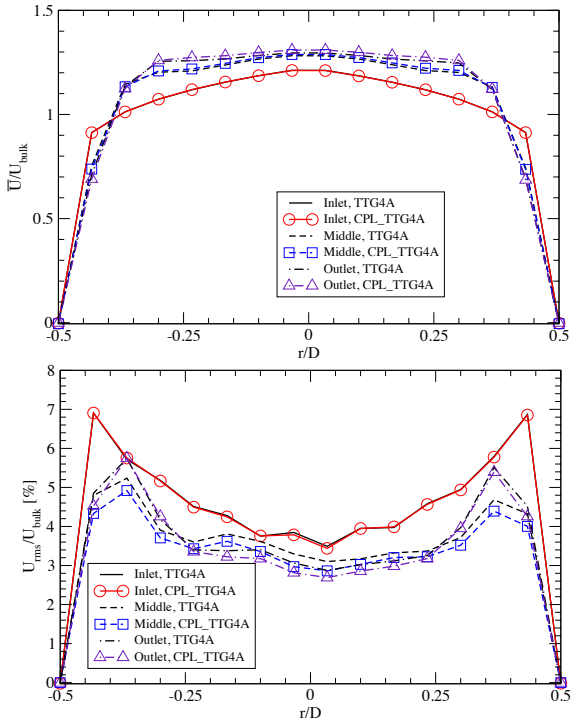

FIGURE 8. Radial mean ($\bar{U}$) and rms (U_{rms}) velocity profiles from coupled (CPL_TTG4A) and standard (TTG4A) simulations, at inlet, middle (coupled interface) and outlet planes respectively.

covers $D/3$ the coupling interface or surface being at $x = 2.5D$. A forced turbulent flow is injected at upstream boundary of the first tube and travels through the pipe before exiting by the right-hand side surface of the second tube. To simulate a moving mesh (although not needed for the type of targeted static configuration), the mesh of the second tube rotates around its central axis at 9500 rpm (revolution per minute). At each time step, the overlapped vertices are hence changing their positions with respect to the first mesh. Note that the problem used for validation is a static turbulent pipe flow so the walls of the entire domain should be fixed at all time, which is ensured by imposing a negative rotating speed at the wall of the rotating pipe.

Looking in details of the predictions (stand alone approach and coupled approach), the instantaneous fields are found to be without any visible distortions at the coupled interface. Figure 8 shows mean statistics from both simulations for the radially dependent axial velocity profiles extracted at the main problem inlet, coupled middle plane and the outlet plane. Extra dissipation is found in the velocity fluctuation profiles for the coupled configuration, which is consistent with the validation case for the traveling vortex. Generally, the radial profiles of the mean velocity and their fluctuations obtained with the coupled simulation are in good agreements with the reference stand alone case confirming the adequacy of the approach for LES.

3 APPLICATIONS

In the following an experimentally diagnosed rotor/stator configuration is simulated using the developed method. The MT1 turbine device is an un-shrouded, full-scale transonic high pressure research turbine established by EU projects TATEF 1 and TATEF 2 and tested in the Isentropic Light Piston Facility by QinetiQ [19, 30]. It consists of 32 stator vanes and 60 rotor blades. Figure 9c shows a schematic view of the geometry: the upstream flow passage, the stator vanes and the rotor blades installed on the hub. At the considered operating condition, the rotational speed of the rotor equals 9,500 rpm, the mass flow rate is 17.4 kg/s and the isentropic Mach number at stator exit is 1.034 yielding a flow Reynolds number of $2.8 \cdot 10^6$ based on the stator chord and stator exit velocity.

Numerical setup

The original ratio of blade counts is 32 : 60. Two configurations are computed in this paper for the demonstration and applicability of the proposed method, shown in Fig. 9 a, b & c, d respectively. The first LES computation consists of 1 scaled stator vane and 2 rotor blades in a 12° sector (Fig. 9a). For this test and to alleviate computational costs, the stator vane is geometrically scaled by a small factor of $32/30$ in order to establish spatial periodicity and maintain the solidity [31]. The scaling technique is proposed and validated by Mayorca *et. al.* [31] and also recently used in U-RANS simulation of the same turbine [32]. Note that scaling techniques are commonly used in unsteady rotor-stator simulations using both RANS approach [31–34] or LES [2]. In a second LES, a geometrically accurate 90° periodic sector configuration (Fig. 9c), with 8 stator vanes and 15 rotor blades, is simulated. The objective of this second exercise is to illustrate the capacity of the method to address full-scale massively parallel computations while providing first insights on the associated computer costs inferred by such tools.

For both computations, the domain consists of two overlapped meshes covering respectively the stator and the rotor. The unstructured hybrid meshes are generated using CENTAUR

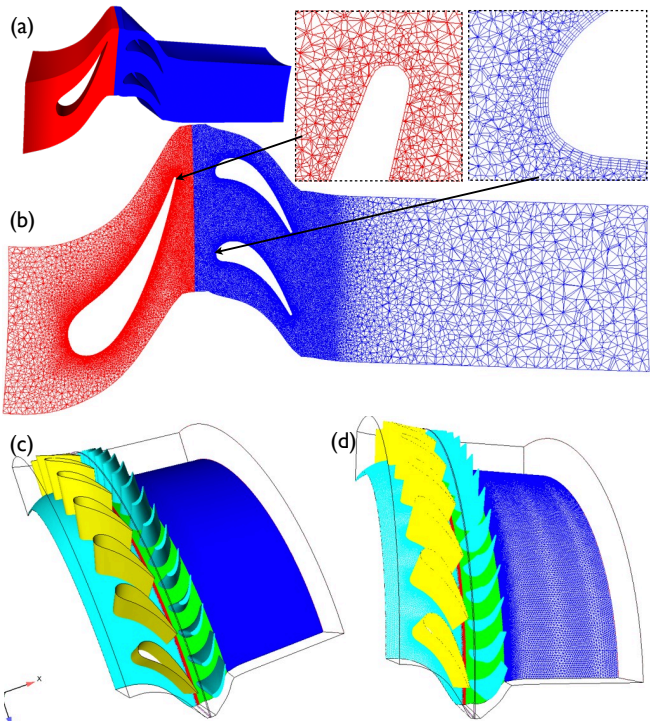

FIGURE 9. Two simulation configurations for QinetiQ MT1 turbine: (1) 12° case with 1 scaled stator and 2 rotors: (a) flow passage with (b) the associated mesh and (2) the 90° case containing 8 stator and 15 rotor blades yielding a quarter sector computational domain of the machine (c) and (d) a view of the associated mesh.

and include a prismatic boundary layer mesh around the vane and blade surfaces while using tetrahedral cells away from these walls. Figure 9b shows some details of the mesh (mainly the 12° configuration). The height of the prismatic layer is constructed based on a normalized wall distance so that $y^+ = 50 \sim 90$ around the blades with an aspect ratio of $\Delta x^+ = \Delta z^+ = 4\Delta y^+$. The mesh size in the overlap region (shown in Fig. 2) is 0.5 mm as in the main flow domain. Similar meshing strategy is used for the 90° configuration, Fig. 9d showing a view of these meshes on the blade and hub walls. The resulting meshes used for the 12° and 90° configurations finally consist of 13 million and 140 million hybrid prism/tetrahedric cells, respectively, Table 1. Although clearly under-resolved for proper LES, these meshes and modeling strategies are still believed relevant for this work where preliminary predictions of a rotor/stator simulation is first investigated with the proposed numerical solution.

Characteristic boundary conditions (NSCBC) [36] are used to avoid problems that might be caused by waves reflecting at these inlet and outlet boundaries. A total pressure, total temperature and the velocity vector angles are prescribed at the inlet. No turbulence fluctuations are imposed on the inflow. The outlet

TABLE 1. Typical parameters used for the two configurations simulated by LES. Note that computational costs are here obtained for one full machine revolution (360°) of the turbine.

Case	Stator+Rotor	No. cells	min y^+	timestep	Iterations	CPU hours
12°	1+2	5M + 8M	50	50ns	126K	4K
90°	8+15	50M + 90M	30	30ns	211K	100K

TABLE 2. Setups for the current LES study and two RANS investigations, together with the experimental operating parameters.

Parameters (unit)	EXP	LES	RANS1 [35]	RANS2 [32]
Rotational speed (rpm)	9500±1%	9500	9500	9500
Inlet: total pressure (bar)	4.6±1%	4.5	4.6	4.615
Inlet: total temperature (K)	444±1%	444	444	444.4
Outlet: static pressure (bar)	1.428±1%	1.428	1.453	1.425
Pressure ratio	3.2	3.15	3.17	3.24
Blade: wall temperature (K)	-	288.5	288.5	-
Blade: min y+	-	50	1-2	20
CFD solver	-	TurboAVBP	elsA	VolSol

of the flow passage is prescribed by targeting a mean static pressure value and a classical logarithmic wall-law boundary condition [37] is imposed on velocity to predict friction of solid walls. As imposed by the configuration, the rotor mesh is rotating by a conventional moving grid method [28], while the rotor blades and the hub of this section are moving walls following the rotating movement. The two lateral surfaces delimiting the sector in the azimuthal direction are axi-periodic boundaries. Details of the boundary conditions are given in Table 2.

LES modeling relies on the standard Smagorinsky SGS model and the LW scheme is used for the computations. Notice that due to the stencil of higher order numerical schemes, such as TTG4A or TTGC requires 4 layers of points each side at the interface. Thus the interpolation costs become more expensive than for LW scheme and needs some optimization in order to maintain acceptable costs for LES applications. Since the LES solver used is fully explicit, the time-step is controlled by the acoustic CFL number. According to the mesh refinement strategies for the 12° and 90° configurations, the time steps are fixed to $\Delta t = 0.5 \cdot 10^{-7}$ s and $\Delta t = 0.3 \cdot 10^{-7}$ s, respectively (Table 1) which results into $126,000$ or $211,000$ iterations for the respective simulations to cover one full revolution of the machine. Associated computational costs are given in Table 1: *i.e.* a full rotation costs about 4 K CPU hours for the 12° configuration and 100 K CPU hours for the 90° configuration. This translates in 8 or 4 days of elapsed wall-clock time if using 512 cores or 1024 cores of a parallel platform to get one full rotation of the 90° configuration.

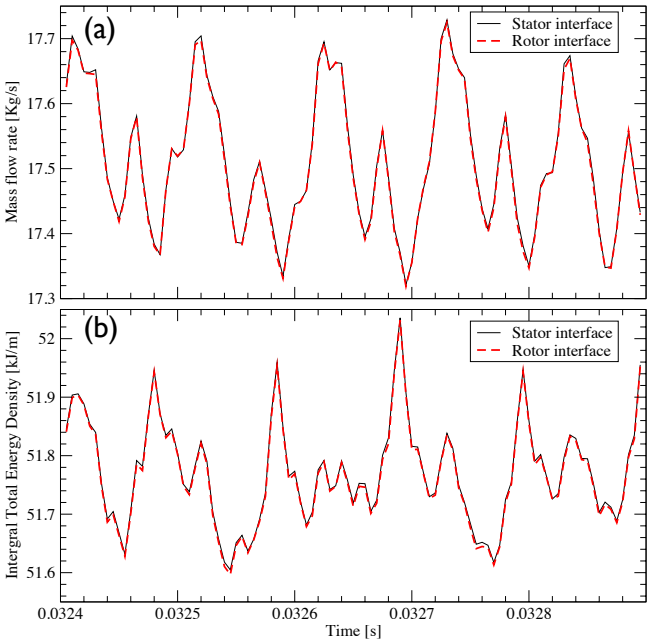

FIGURE 10. The evolutions of integrated (a) mass flow rates $\int \rho u \cdot ds$ and (b) total energy density $\int \rho E \cdot ds$ over the coupled middle planes at stator and rotor sides.

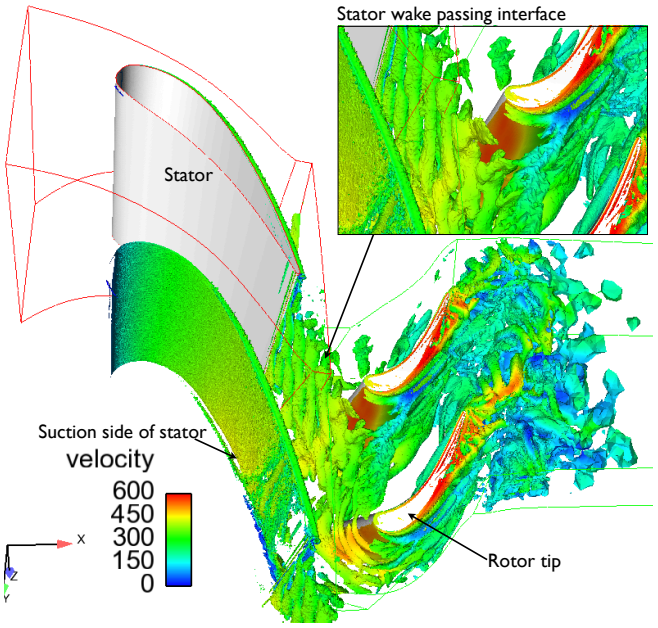

FIGURE 11. Q-criterion iso-surface showing vortex structure colored by velocity magnitude.

Results

As indicated in the methodology, interpolation is introduced which can threaten the conservative properties of the simulation in complex geometries and flows, although preliminary test cases did not exhibit such issues. Prior to the analysis of the LES predictions of MT1, the flow conservation property must first be checked. Figure 10a shows the temporal evolutions of the integrated mass flow rates through the coupled interface located between the stator part and the rotor for the 12° configuration. The two depicted curves of the mass flow rate corresponding to the fixed grid interface and its rotating counterpart are perfectly matching, which indicates good conservation properties on the mass flow. As indicated by Fig. 10a, this quantity may be evolving with time over around the mean operating value of 17.5 kg/s indicating the interaction at the interface of the rotor and stator flows. The evolutions of the integrated values of total energy density over the coupled interfaces are given in Fig. 10b, which confirms good energy conservation of the coupled simulation.

LES provides access to a fully unsteady description of the main flow around the blade, as illustrated by the preliminary flow topologies obtained by the proposed coupled strategy. Multiple diagnostics are available and Fig. 11 shows an instantaneous iso-surfaces of the Q-criterion. The value of Q-criterion is chosen to show the main turbulent structures. The main pattern visible here is the stator wake which is at this instant impinging on the leading edge of one of the rotor blade. This stator wake is rapidly de-structured and exhibits vortex shedding and pass through the coupling interface without any visible interference, due to interpolation for example. On the stator suction side, the iso-surface reveals a shock-induced boundary layer separation in the near trailing edge region of the blade. Figure 12 pictures a radial plane located at middle height span of an instantaneous field of vorticity magnitude that confirms the $3D$ view of the stator wake, the generation of the periodic vortical structures (Karman street) and their interaction with the rotor blades. In this view, the flow passage (1 stator and 2 rotors) is periodically duplicated for better analysis. As anticipated in the discussion, vortex shedding is generated at the trailing edge of the stator where the boundary layers separate from the wall and is then convected by the flow downstream into the rotor passage. Figure 13 shows instantaneous contours of the absolute Mach number at two times of the rotation in the previous plane. At the rotor/stator interface, the flow field is clearly evolving due to the change in relative position of the rotor blades with respect to the stator vane. Depending on this relative position, transonic flow pockets issued on the stator side evolve and move with time as shown by the isoline of Mach $= 1$ on Fig. 13.

Focusing now on the flow field in the rotor, Figs. 11- 13, the stator wake is seen to penetrate the rotor blades and evolves differently in the pressure and suction sides. The flow structures entering on the suction side are rapidly distorted by the flow, mainly because of the flow acceleration in this region. These structures are hence elongated and remain in the near blade boundary layer

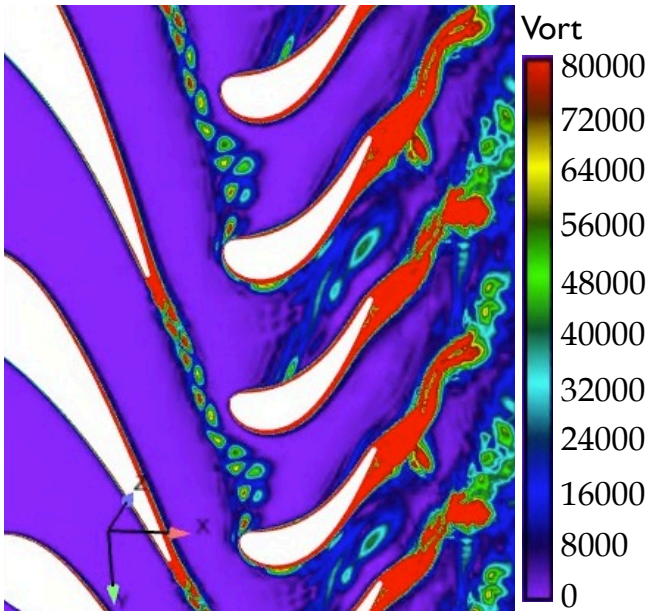

FIGURE 12. Instantaneous vorticity magnitude field at the rotor/stator stage.

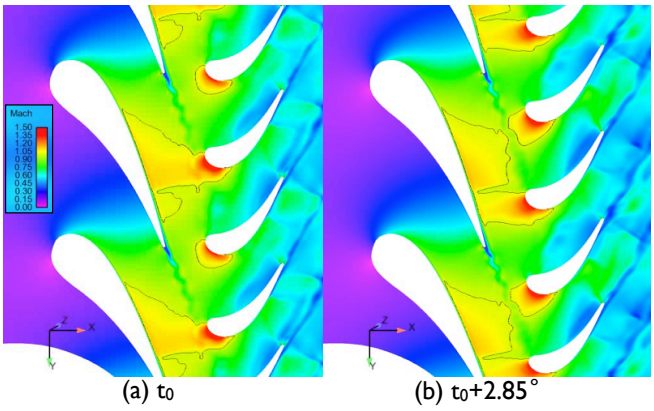

FIGURE 13. Instantaneous fields of absolute Mach number ($H = 50\%$). Iso-lines represent the Mach= 1.

region. On the pressure side, the coherence and existence of the stator Karman street is much less affected. Indeed the structures penetrate the entire section of the passage and are eventually convected downstream all the way to the rotor wake, Fig. 12. Series illustrations of normalized magnitude of the density gradient ($|\nabla\rho|/\rho$, corresponding to Schlieren image) are shown in Fig. 14 at different instants of the stator passing frequency and out of the 12° simulation. In this reference frame, the incoming wake of the stator (denoted as **I** in Fig. 14) is periodically brushing the rotor passage as underlined in the previous discussion. One strong

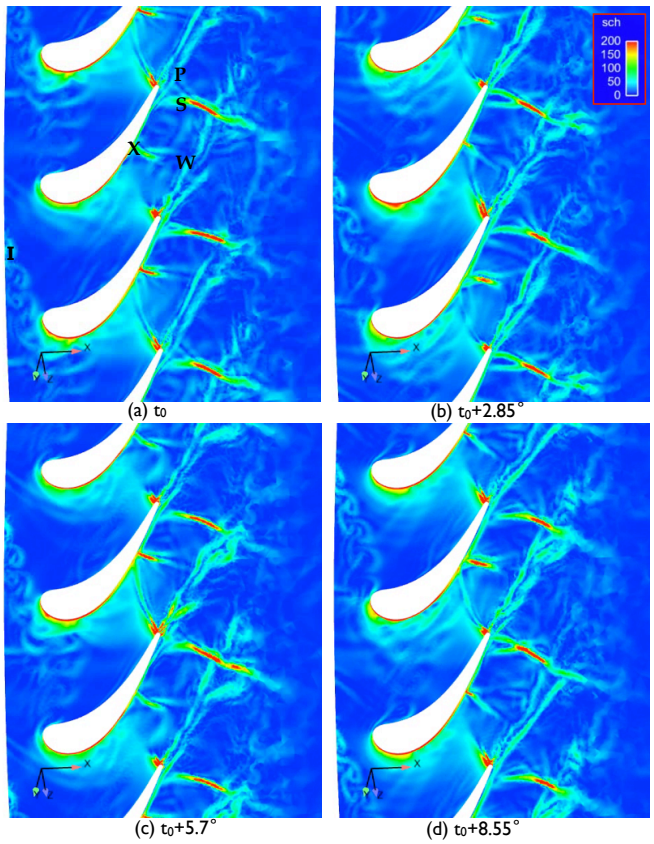

FIGURE 14. A sequential fields of $|\nabla\rho|/\rho$ ($H = 50\%$) from local viewpoint of the rotor. The period for stator passage is 12°.

shock (**S**), also evidenced by RANS computations [32, 35], is found by the LES near the trailing edge of the blade. A second shock (noted **x**) is also captured on the suction side. This second shock is weaker and seems to be highly influenced by the incoming stator wake passing frequency discussed above. Time series analysis for a probe positioned close to **x**, Fig. 15b, shows pressure variations between 0.95 and 1.45 bars. The frequency (Fig. 15a) approaches 4750 Hz, and coincides with the stator passage frequency. Note also that this shock induces a periodic suction side boundary layer separation, **P**, evidenced in Fig. 14.

In order to proceed with the validation of such simulations against measurements, two full revolutions of the 12° configuration are conducted out of which only a part of the second revolution is time averaged to retrieve statistics: *i.e.* 50,000 iterations (about 140° of rotation). Results are then compared to experimental data as well as one RANS [35] and one Unsteady RANS (U-RANS) [32] prediction, respectively noted RANS1and RANS2 for which the numerical setups are detailed in Table 2. The RANS1 case was simulated using a structure mesh with 2.6M points ($y+ : 1 \sim 2$) for one stator passage and

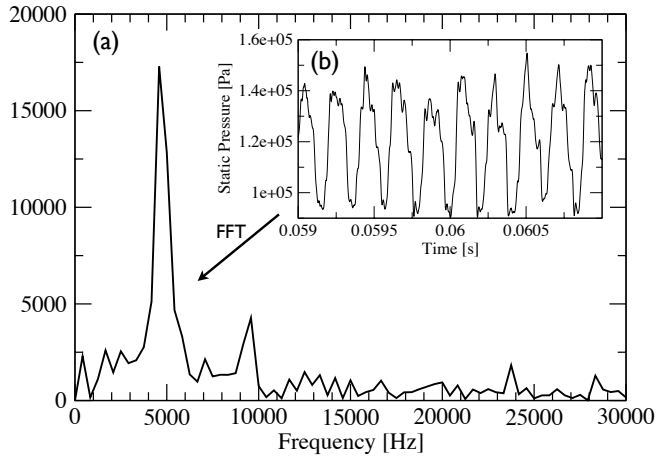

FIGURE 15. Pressure signals at probe **X** (in Fig. 14): (a) the spectrum profiles and (b) temporal evolution of the signal.

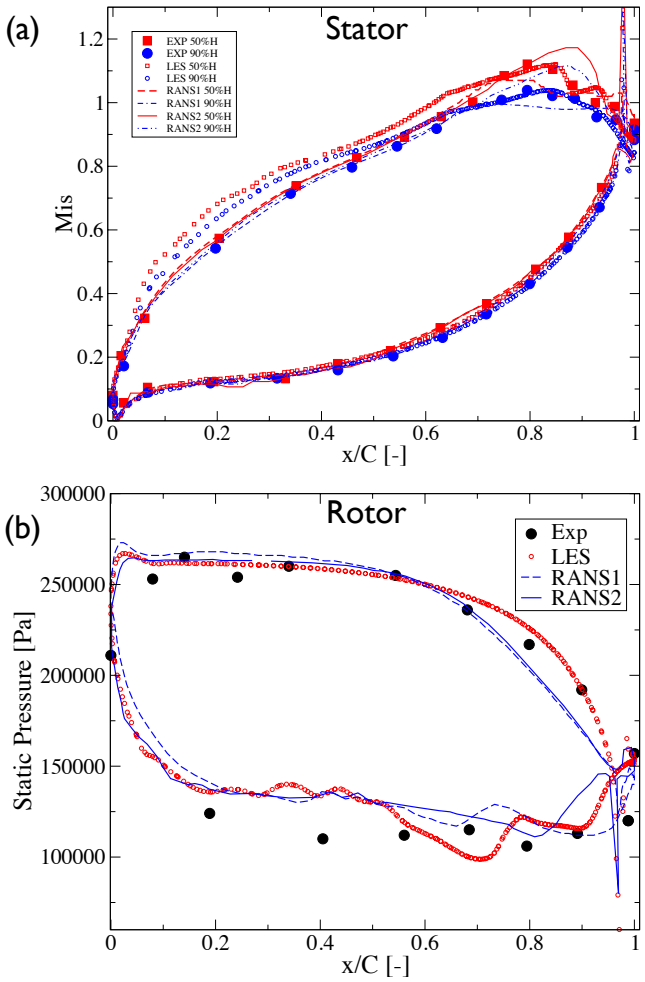

FIGURE 16. Mean profile numerical predictions at different spanwise locations of the blades: (a) isentropic Mach number at 50% and 90% of the stator blade and (b) static pressure at 50% span of the rotor blade. RANS1 denotes a steady wall-resolved RANS computation [35] and RANS2 denotes a wall-modeled Unsteady RANS [32].

one rotor passage. The unsteady RANS case (RANS2) was simulated using a structured mesh with y+ from 20 to 200, based on the geometrically scaled setup [32] of one stator passage and two rotor passages. Figure 16a & b shows the mean isentropic Mach number evolutions at two span heights (50% and 90%) along a) a stator and b) a rotor blade. All simulations are quite consistent with the experiments over the pressure side of both blades. On the suction side of the stator, Fig. 16a, close to the trailing edge ($x/C = 0.8$), LES results (denoted by small empty symbols) are in good agreements with experimental data, while RANS1 and RANS2 results (denoted by lines) are underestimate or overestimate the experimental findings. Note however that room of improvement is clearly present in the LES simulation, as evidenced on the suction side ($x/C = 0.1$ to $x/C = 0.7$) where the law of the wall approach or the wall resolution show clear limitations in representing the boundary layer state. The turbulence intensity, which is currently missing, is also mandatory to correctly predict the boundary layer transitions [5, 6, 38]. As a result, injecting the experimental inlet turbulence (also require better grid resolutions on inlet block [38]) is crucial to better capture more physics at the stator suction side.

Mean static pressure profiles at mid-span of the rotor blade are given in Fig. 16b. For this blade, LES and RANS results are in reasonable agreement with experiments. LES predictions are clearly better than RANS in pressure sides of the blade. Improvements are nonetheless needed for the suction side predictions. Again wall modeling and grid resolution are the preliminary directions for future investigation. However, both wall-resolved RANS [35] and wall-modeled URANS [32] have the similar discrepancy between the experimental data on rotor suction side.

Figure 17 shows azimuthal mean profiles in a near rotor-exit plane where data for the yaw angle and total pressure were obtained experimentally. All simulations are qualitatively in good agreement with experimental measurements although a clear deficit is evidenced in the ability of the proposed LES setup to properly capture the tip clearance effects at 90% span. Current mesh resolution is rather poor at tip-gap (gap size $\sim$ 0.6 mm) with only 6 $\sim$ 7 layers of cells across. Following the pioneering work of You *et. al.* [7], efforts are required to refine the tip-gap region's mesh for better predictions of tip-clearance vortical structures, which may strongly affect the predictions of flow direction close to the rotor tip (see Fig. 17b).

Finally preliminary predictions of the flow fields issued by the 90° LES configuration are provided on Fig. 18. These instantaneous views of the vorticity magnitude and density Schlieren

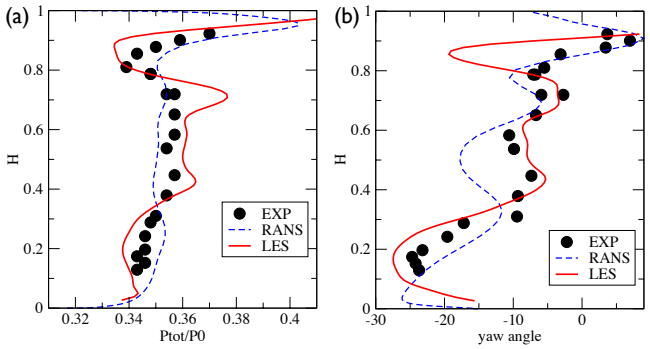

FIGURE 17. Azimuthal mean profiles of total pressure (left) and yaw angle (right) at a rotor exiting near-plane. Total pressure is normalized using $P_0 = 4.6 \cdot 10^6 Pa$.

owe to be compared with the predictions from the 12° configuration of Figs. 12 & 14 respectively. Mean spatial features are in agreement for both computations confirming the feasibility of such LES with the proposed methodology.

4 CONCLUSIONS

An in-house code (called TurboAVBP) is developed for LES of turbomachinery by coupling multi-copies of an unstructured compressible LES solver developed by CERFACS and IFP-EN (AVBP). In the proposed strategy the rotor/stator interface is treated via a coupling method based on the overset grid method. In the specific context of LES, this rotating interface is exposed to numerical difficulties which may corrupt the high fidelity requirements of this modelling approach. To ensure that the method is adequate for LES, several numerical test cases are proposed, with an increasing degree of complexity, to evaluate the solution. From these tests, the coupling method is proven to handle acoustics, vortices and turbulence with an acceptable degree of accuracy for LES. The strategy also shows itself to be quite successful especially considering the room for possible numerical improvements, in the interpolation procedure for example.

Based on these results, the approach is then applied to the QinetiQ MT1 high-pressure transonic experimental turbine to illustrate the potential of rotor/stator LES. Although clearly underresolved in terms of local grid resolution or wall modeling, mean LES statistics prove to be in reasonable agreement with experimental data and these predictions appear to be very competitive, if compared to the traditional RANS or URANS approach. The inherently unsteady in nature of LES allows capturing many flow features otherwise difficult to anticipate. Of course, computational costs are much larger with such tools. Improvements are possible vie tabulation of interpolation information or further to take advantage of the ever increasing massively parallel computers. In parallel, such tools underline the need for high-order

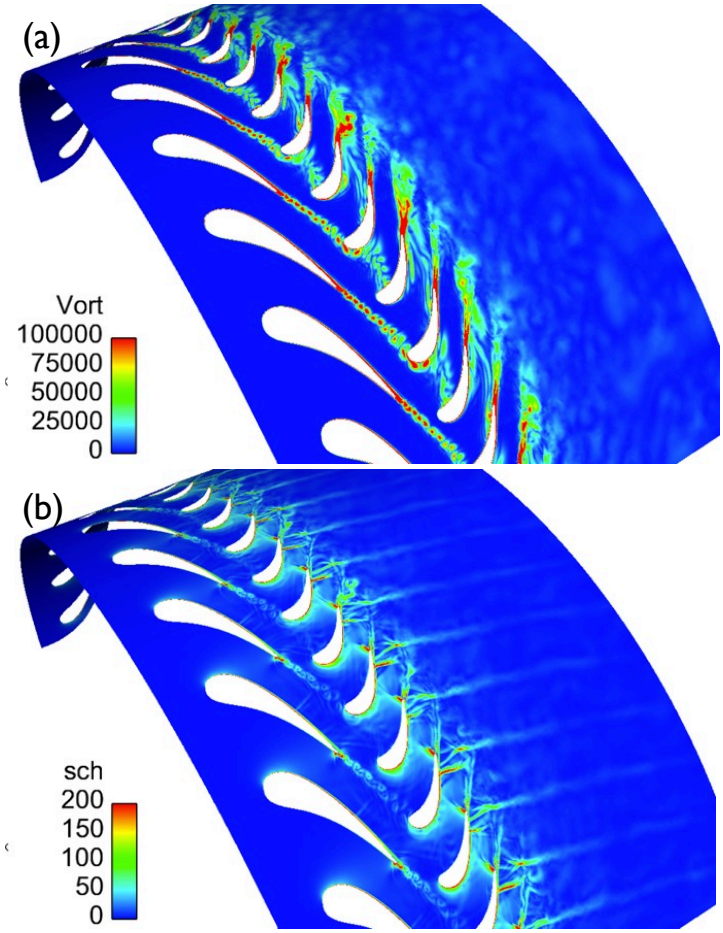

FIGURE 18. Instantaneous fields of the vorticity magnitude (a) and $|\nabla\rho|/\rho$ (b) as obtained from the 90° LES prediction (H=50%).

interpolation algorithms for unstructured meshes. And the feasibility of such simulations with better grid resolutions or using more advanced wall models [39, 40] should also be tested for turbomachinery simulations.

Acknowledgments

The authors would like to thank the foundation of Sciences et Technologies pour l'Aéronautique et l'Espace RTRA project COEFFCI for its financial support and acknowledge the kindest help from O. Vermorel, M. Montagnac and G. Staffelbach from the CERFACS CFD team and the helpful comments from S. Moreau (Université de Sherbrooke) and L. Pons (TURBOMECA).

REFERENCES

[1] Menzies, K., 2009. "Large eddy simulation applications in gas turbines". *Philos Transact A Math Phys Eng Sci.,* ***367***(1899), pp. 2827–2838.

[2] McMullan, W., and Page, G., 2012. "Towards large eddy simulation of gas turbine compressors". *Progress in Aerospace Sciences,* ***52***(0), pp. 30 – 47.

[3] Tucker, P., 2011. "Computation of unsteady turbomachinery flows: Part 2 "les and hybrids". *Progress in Aerospace Sciences,* ***47***(7), pp. 546 – 569.

[4] Bhaskaran, R., and Lele, S. K., 2010. "Large eddy simulation of free-stream turbulence effects on heat transfer to a high-pressure turbine cascade". *Journal of Turbulence,* ***11***(6), pp. 1–15.

[5] Collado-Morata, E., Gourdain, N., Duchaine, F., and Gicquel, L., 2012. "Effects of free-stream turbulence on high pressure turbine blade heat transfer predicted by structured and unstructured les". *International Journal of Heat and Mass Transfer,* ***55***(21-22), pp. 5754 – 5768.

[6] G. Medic, J. Joo, S. L., and Sharma, O., 2012. "Prediction of heat transfer in a turbine cascade with high levels of free-stream turbulence". In Proceeding of the Summer Program Center for Turbulence Research, NASA AMES - Stanford University, USA.

[7] You, D., Wang, M., Moin, P., and Mittal, R., 2007. "Large-eddy simulation analysis of mechanisms for viscous losses in a turbomachinery tip-clearance flow". *Journal of Fluid Mechanics,* ***586***, pp. 177–204.

[8] Moureau, V., 2011. "Design of a massively parallel cfd code for complex geometries". *Comptes Rendus Mécanique,* ***339***, pp. 141–148.

[9] Tucker, P., 2011. "Computation of unsteady turbomachinery flows: Part 1 "progress and challenges". *Progress in Aerospace Sciences,* ***47***(7), pp. 522 – 545.

[10] Boileau, M., Staffelbach, G., Cuenot, B., Poinsot, T., and Barat, C., 2008. "Les of an ignition sequence in a gas turbine engine". *Combustion and Flame,* ***154***(1-2), pp. 2 – 22.

[11] Gicquel, L., Staffelbach, G., and Poinsot, T., 2012. "Large eddy simulations of gaseous flames in gas turbine combustion chambers". *Progress in Energy and Combustion Science,* ***38***(6), pp. 782 – 817.

[12] Bodony, D. J., Zagaris, G., Reichert, A., and Zhang, Q., 2011. "Provably stable overset grid methods for computational aeroacoustics". *Journal of Sound and Vibration,* ***330***(17), pp. 4161 – 4179.

[13] Desquesnes, G., Terracol, M., Manoha, E., and Sagaut, P., 2006. "On the use of a high order overlapping grid method for coupling in cfd/caa". *J. Comput. Phys.,* ***220***(1), Dec., pp. 355–382.

[14] Sherer, S. E., and Scott, J. N., 2005. "High-order compact finite-difference methods on general overset grids". *Journal of Computational Physics,* ***210***(2), pp. 459 – 496.

[15] Sengupta, T. K., Suman, V., and Singh, N., 2010. "Solving navier-stokes equation for flow past cylinders using single-block structured and overset grids". *Journal of Computational Physics,* ***229***(1), pp. 178 – 199.

[16] Steger, J., Dougherty, F., and Beneck, J., 1982. "A chimera grid scheme". *ASME Mini-Symposium on Advances in Grid Generation*.

[17] Benjamin Francois, Michel Costes, G. D., 2011. "Comparison of chimera and sliding mesh techniques for unsteady simulations of counter rotating open-rotors". In ISABE-2011-1231.

[18] Rai, M. M., 1987. "Navier-stokes simulations of rotor/stator interaction using patched and overlaid grids". *Journal of Propulsion and Power,* ***3***(5), pp. 387–396.

[19] Hilgenfeld, L., and Pfitzner, M., 2004. "Unsteady boundary layer developement due to wake passing effects on a highly loaded linear compressor cascade". *J. Turbomach.,* ***126***, pp. 493–500.

[20] Schonfeld, T., and Rudgyardt, M., 1999. "Steady and unsteady flow simulations using the hybrid flow solver avbp". *AIAA Journal,* ***37***, pp. 1378–1385.

[21] Lax, P. D., and Wendroff, B., 1964. "Difference schemes for hyperbolic equations with high order of accuracy". *Communications on pure and applied mathematics,* ***17***, pp. 381–398.

[22] Selmin, V., 1987. Third order finite element schemes for the solution of hyperbolic problems. Tech. rep., INRIA.

[23] Colin, O., and Rudgyard, M., 2000. "Development of high-order taylor-galerkin schemes for unsteady calculations". *Journal of Computational Physics,* ***162***(2), pp. 338–371.

[24] Lekien, F., and Marsden, J., 2005. "Tricubic interpolation in three dimensions". *International Journal for Numerical Methods in Engineering,* ***63***(3), pp. 455–471.

[25] Piacentini, A., Morel, T., Thevenin, A., and Duchaine, F., 2011. "Open-palm an open source dynamic parallel coupler". In Coupled Problems 2011.

[26] CNGS-Steering-Committee, 2007. The cfd general notation system standard interface data structures. Tech. rep., http://cgns.org.

[27] Ern, A., and Guermond, J.-L., 2003. *Theory and Practice of Finite Elements*. Springer.

[28] Moureau, V., Lartigue, G., Sommerer, Y., Angelberger, C., Colin, O., and Poinsot, T., 2005. "Numerical methods for unsteady compressible multi-component reacting flows on fixed and moving grids". *Journal of Computational Physics,* ***202***(2), pp. 710 – 736.

[29] Visbal, M. R., and Gaitonde, D. V., 1999. "High-order-accurate methods for complex unsteady subsonic flows". *AIAA Journal,* ***37***(10), pp. 1231–1239.

[30] I. Qureshi, T. Povey, A. D. S., and Chana, K. S., 2010. "Effect of temperature nonuniformity on heat transfer in

an unshrouded transonic hp turbine: An experimental and computaional investigation". *ASME Turbo Expo GT2010-22700*.

[31] Mayorca, M. A., Andrade, J. A. D., Vogt, D. M., Martensson, H., and Fransson, T. H., 2009. "Effect of scaling of blade row sectors on the prediction of aerodynamic forcing in a highly-loaded transonic compressor stage". *ASME TURBO EXPO GT2009-59601*.

[32] Hosseini, S. M., Fruth, F., Vogt, D. M., and Fransson, T. H., 2011. "Effect of scaling of blade row sectors on the prediction of aerodynamic forcing in a highly-loaded transonic turbine stage". *ASME TURBO EXPO GT2011-45813*.

[33] Rai, M. M., 1990. "Multi-airfoil navier-stokes simulations of turbine rotor-stator interaction". *ASME Journal of Turbomachinery,* ***112***, pp. 377–396.

[34] Clark, J. P., Stetson, G. M., Magge, S. S., Ni, R. H., Jr, C. W. H., and Dunn, M. G., 2000. "The effect of airfoil scaling on the predicted unsteady loading on the blade of a 1 and 1/2 stage transonic turbine and a comparison with experimental results". *ASME TURBO EXPO 2000-GT-0446*.

[35] Pichon, T. L., 2008. Modélisation aérodynamique et aérothermique externe des aubages de turbines axiales avec le code elsa. Tech. rep., TURBOMECA.

[36] Poinsot, T., and Lele, S., 1992. "Boundary conditions for direct simulations of compressible viscous flows". *Journal of Computational Physics,* ***101***(1), pp. 104 – 129.

[37] P. Schmitt, T. Poinsot, B. S., and Geigle, K. P., 2007. "Large-eddy simulation and experimental study of heat transfer, nitric oxide emissions and combustion instability in a swirled turbulent high-pressure burner". *Journal of Fluid Mechanics,* ***570***, p. 1746.

[38] Medic, G., and Sharma, O., 2012. "Large-eddy simulation of flow in a low-pressure turbine cascade". *ASME Turbo Expo GT2012-68878*.

[39] Bocquet, S., Sagaut, P., and Jouhaud, J., 2012. "A compressible wall model for large-eddy simulation with application to prediction of aerothermal quantities". *Physics of Fluids,* ***24***(065103).

[40] Maheu, N., Moureau, V., Domingo, P., Duchaine, F., and Balarac, G., 2012. "Large-eddy simulations of flow and heat transfer around a low-mach number turbine blade". In Proceeding of the Summer Program Center for Turbulence Research, NASA AMES - Stanford University, USA.